Available at
http://pvamu.edu/aam
Appl. Appl. Math.
ISSN: 1932-9466

Applications and Applied Mathematics:
An International Journal
(AAM)

Vol. 14, Issue 2 (December 2019), pp. 687 – 698

Understanding the Fundamental Molecular Mechanism of Osteogenic Differentiation from Mesenchymal Stem Cells

[1]Imelda Trejo and [2]Hristo V. Kojouharov

Department of Mathematics
The University of Texas at Arlington
Arlington, TX 76019-0408, USA
[1]imelda.trejo@mavs.uta.edu; [2]hristo@uta.edu

Received: July 17, 2019; Accepted: September 19, 2019

Abstract

A mathematical model is presented to study the regulatory effects of growth factors in osteoblastogenesis. The model incorporates the interactions among mesenchymal stem cells, osteoblasts, and growth factors. The resulting system of nonlinear ordinary differential equations is studied analytically and numerically. Mathematical conditions for successful osteogenic differentiation and optimal osteoblasts population are formulated, which can be used in practice to accelerate bone formation. Numerical simulations are also presented to support the theoretical results and to explore different medical interventions to enhance osteoblastogenesis.

Keywords: Bone fracture healing; Growth factors; Hopf bifurcation; Mesenchymal stem cell differentiation; Osteoblasts; Osteogenesis; Stability

MSC 2010 No.: 34C23, 34C25, 34D20, 92B05, 92C37, 92C50, 92C40

1. Introduction

The differentiation of mesenchymal stem cells (MSCs) into osteoblasts is a fundamental process in bone formation as osteoblasts build up the bone tissue matrix through their released collagen (Doblaré et al. (2004), Florencio-Silva et al. (2015)). This process is mediated by different extracellular signals including mechanical loads and molecular factors (Dimitriou et al. (2005), Ghiasi et

al. (2017)). Particularly, specific growth factors such as the bone morphogenetic proteins (BMPs) and transforming growth factor-β (TGF-β) activate and direct the differentiation of MSCs into osteoblasts (Garg et al. (2017), Wu et al. (2016), Fakhry et al. (2013)). Consequently, growth factors are promising therapeutic agents for the initiation and enhancement of bone fracture healing, among other biological process (Devescovi et al. (2008), Fakhry et al. (2013)).

Several mathematical models have been recently developed to study the dynamics among the MSCs, osteoblasts, and growth factors to predict bone development over time (Bailon-Plaza and Van Der Meulen (2001), Carlier et al. (2015), Moreo et al. (2009), Trejo et al. (2019)). However, none of them have analyzed theoretically the growth factors regulation of MSCs differentiation toward osteoblasts (Ghiasi et al. (2017)). In this paper, the model developed in Bailon-Plaza and Van Der Meulen (2001) is modified to closely examine the important dynamics among the MSCs, osteoblasts, and TGF-β, which allows for a greater insight of the regulatory effects of the growth factors directing the differentiation of the MSCs into osteoblasts. Based on the presented analysis of the new model, a threshold value of the growth factor concentration, the existence of which was only hypothesized in Bailon-Plaza and Van Der Meulen (2001), is explicitly determined to guarantee a successful osteoblastogenesis.

The paper is organized as follows. In Section 2, the mathematical model is formulated. The stability analysis of the model is presented in Section 3. Bifurcations for the model are discussed in Section 4. In Section 5, numerical simulations are performed to validate the theoretical findings. It also demonstrates the functionality of the model by numerically simulating the progression of the osteoblastogenesis process. The discussion and conclusion are presented in Section 6.

2. Mathematical Model

Figure 1 illustrates a flow diagram for the cellular and molecular dynamics during osteoblastogenesis, where the main assumption is that the osteogenic differentiation is conducted by the interactions among the MSCs (C_m), osteoblasts (C_b), and the TGF-β (g_b). The cells and cellular dynamics are represented by the circular shapes and solid arrows. The g_b concentration and its production/decay are represented by the octagonal shape and dashed/solid arrows. The activation of the osteogenic differentiation is represented by the solid compound arrow.

The osteogenic differentiation is modeled with a mass-action system of nonlinear ordinary differential equations, where all variables represent homogeneous quantities in a given volume. Following the flow diagram given in Figure 1 yields the resulting system of equations:

$$\frac{dC_m}{dt} = k_{pm}C_m\left(1 - \frac{C_m}{K_{lm}}\right) - d_m g_b C_m, \tag{1}$$

$$\frac{dC_b}{dt} = k_{pb}C_b\left(1 - \frac{C_b}{K_{lb}}\right) + d_m g_b C_m - d_b C_b, \tag{2}$$

$$\frac{dg_b}{dt} = k_{gb}C_b - d_g g_b. \tag{3}$$

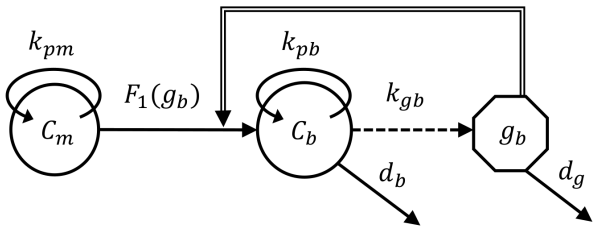

Figure 1. Flow diagram of the osteogenic differentiation process: MSCs (C_m) proliferate and differentiate into osteoblasts. Osteoblasts (C_b) proliferate and differentiate into osteocytes. Transforming growth factor-β (g_b) is synthesized by the osteoblasts, it activates the osteogenic differentiation, and decays

Equation (1) describes the rate of change with respect to time of C_m. It increases due to a constant cellular division, at a rate k_{pm}, up to a constant-maximal carrying capacity, K_{lm}. It decreases by differentiation, where the differentiation rate is regulated by g_b. This regulation is modeled with a linear function, i.e., $F_1(g_b) = d_m g_b$. Equation (2) describes the rate of change with respect to time of C_b. It increases when MSCs differentiate into osteoblasts or when osteoblasts proliferate. Osteoblasts proliferate at a constant rate, k_{pb}, up to a constant-maximal carrying capacity, K_{lb}. The osteoblasts density decreases at a constant rate d_b when osteoblasts differentiate into osteocytes. Equation (3) describes the rate of change with respect to time of g_b, which increases due to production by C_b, and decreases by degradation.

3. Model Analysis

The analysis of Model (1)-(3) is done by finding the equilibria, denoted by $E(C_m, C_b, g_b)$, and their corresponding stability properties. Setting the right-hand sides of the equations (1)-(3) equal to zero yields the following four equilibria: $E_0(0,0,0)$, $E_1(K_{lm},0,0)$, $E_2(0,C^*_{b_2},g^*_{b_2})$, and $E_3(C^*_{m_3},C^*_{b_3},g^*_{b_3})$. Note that E_0 and E_1 represent unsuccessful osteoblastogenesis due to the absence of osteoblasts, while E_2 and E_3 represent successful outcomes, since the osteoblasts remain at positive constant densities. Table 1 summarizes the equilibria and their corresponding existence and stability conditions.

Table 1. Existence and stability conditions for the equilibrium points

Equilibrium Points	Existence	Stability
$E_0(0,0,0)$	always	always unstable
$E_1(K_{lm},0,0)$	always	$d_b > k_{pb} + d_m k_{gb} K_{lm}/d_g$
$E_2(0,C^*_{b_2},g^*_{b_2})$	$d_b < k_{pb}$	$d_b < k_{pb}\left(1 - d_g k_{pm}/d_m k_{gb} K_{lb}\right)$
$E_3(C^*_{m_3},C^*_{b_3},g^*_{b_3})$	$k_{pb}\left(1 - d_g k_{pm}/d_m k_{gb} K_{lb}\right) < d_b < k_{pb} + d_m k_{gb} K_{lm}/d_g$	$b_1 b_2 - b_3 > 0$

The existence conditions of each equilibrium point arise from the fact that all biologically meaningful variables are non-negative, and the stability is analyzed using the Jacobian of the system (1)-(3) at each equilibrium point and finding its corresponding eigenvalues (Wiggins (2003)) as discussed in the following theorems:

Theorem 3.1.

The equilibrium $E_0(0,0,0)$ exists for all parameter values of the model and it is unstable.

Proof:

The elements of E_0 are non-negative for all parameter values of the model. Hence, E_0 is a biologically feasible equilibrium. The Jacobian matrix $J(E_0)$ is given by the following lower-triangular matrix:

$$J(E_0) = \begin{pmatrix} k_{pm} & 0 & 0 \\ 0 & k_{pb} - d_b & 0 \\ 0 & k_{gb} & -d_g \end{pmatrix}.$$

Since the eigenvalue $\lambda_{C_m} = k_{pm} > 0$, then E_0 is unstable. ∎

Theorem 3.2.

$E_1(K_{lm}, 0, 0)$ exists for all parameter values and is locally stable if and only if $d_b > k_{pb} + d_m k_{gb} K_{lm}/d_g$.

Proof:

E_1 is a biologically feasible equilibrium for all parameter values of the model since its elements are always nonnegative. The Jacobian matrix $J(E_1)$ is as follows:

$$J(E_1) = \begin{pmatrix} -k_{pm} & 0 & -d_m K_{lm} \\ 0 & k_{pb} - d_b & d_m K_{lm} \\ 0 & k_{gb} & -d_g \end{pmatrix}.$$

Hence, the characteristic polynomial of $J(E_1)$ is given by $p(\lambda) = (\lambda + k_{pm})(\lambda^2 + a_1\lambda + a_0)$, where $a_1 = d_g + (d_b - k_{pb})$ and $a_0 = d_g(d_b - k_{pb}) - d_m k_{gb} K_{lm}$. By hypothesis $d_b - k_{pb} > d_m k_{gb} K_{lm}/d_g > 0$, therefore, $a_0 > 0$ and $a_1 > 0$. By the Routh-Hurwitz criteria, $n = 2$, the roots of $\lambda^2 + a_1\lambda + a_0$ are negative or have negative real parts, which implies that E_1 is locally stable. ∎

Theorem 3.3.

$E_2(0, C^*_{b_2}, g^*_{b_2})$ exists if $k_{pb} > d_b$ and it is stable if and only if $k_{pb} > d_b + d_g k_{pb} k_{pm}/d_m k_{gb} K_{lb}$, where

$$C^*_{b_2} = K_{lb}(1 - d_b/k_{pb}), \quad \text{and} \quad g^*_{b_2} = k_{gb} C^*_{b_2}/d_g.$$

Proof:

By hypothesis $k_{pb} > d_b$, hence, both $C^*_{b_2}$ and $g^*_{b_2}$ are positive, and therefore, E_2 is a biologically feasible equilibrium. The Jacobian matrix $J(E_2)$ is given by the following lower-triangular matrix:

$$J(E_2) = \begin{pmatrix} k_{pm} - d_m g^*_{b_2} & 0 & 0 \\ d_m g^*_{b_2} & -k_{pb} + d_b & 0 \\ 0 & k_{gb} & -d_g \end{pmatrix}.$$

Since $k_{pm} - d_m g^*_{b_2} = (d_g k_{pb} k_{pm} - d_m k_{gb} K_{lb}(k_{pb} - d_b))/d_g k_{pb}$, then, by hypothesis, it implies that $k_{pm} - d_m g^*_{b_2} < 0$. Hence, all the eigenvalues of $J(E_2)$ are negative, and therefore, E_2 is locally stable. ■

Theorem 3.4.

$E_3(C^*_{m_3}, C^*_{b_3}, g^*_{b_3})$ exists if

$$k_{pb}\,(1 - d_g k_{pm}/d_m k_{gb} K_{lb}) < d_b < k_{pb} + d_m k_{gb} K_{lm}/d_g,$$

where

$$C^*_{m_3} = \frac{k_{pm}}{\Delta}\left(\frac{k_{pb}}{K_{lb}} + \frac{d_m k_{gb}(d_b - k_{pb})}{d_g k_{pm}}\right), \quad C^*_{b_3} = \frac{k_{pm}}{\Delta}\left(\frac{d_m k_{gb}}{d_g} + \frac{k_{pb} - d_b}{K_{lm}}\right),$$

$$g^*_{b_3} = \frac{k_{gb} k_{pm}}{d_g\,\Delta}\left(\frac{d_m k_{gb}}{d_g} + \frac{k_{pb} - d_b}{K_{lm}}\right), \quad \text{with} \quad \Delta = \left(\frac{d_m k_{gb}}{d_g}\right)^2 + \frac{k_{pm} k_{pb}}{K_{lm} K_{lb}}.$$

Furthermore, E_3 is locally stable if $b_1 b_2 - b_3 > 0$, is unstable if $b_1 b_2 - b_3 < 0$, and is a non-hyperbolic equilibrium point if $b_1 b_2 - b_3 = 0$, where b_1, b_2, b_3 are defined as follows:

$$\begin{aligned} b_1 &= \frac{k_{pm} C^*_{m_3}}{K_{lm}} + \frac{k_{pb} C^*_{b_3}}{K_{lb}} + \frac{d_m k_{gb} C^*_{m_3}}{d_g} + d_g, \\ b_2 &= \frac{k_{pm} C^*_{m_3}}{K_{lm}}\left(\frac{k_{pb} C^*_{b_3}}{K_{lb}} + \frac{d_m k_{gb} C^*_{m_3}}{d_g} + d_g\right) + d_g \frac{k_{pb} C^*_{b_3}}{K_{lb}}, \\ b_3 &= d_g \Delta C^*_{m_3} C^*_{b_3}. \end{aligned} \tag{4}$$

Proof:

For the first statement of the theorem, notice that the $C^*_{m_3}$ and $C^*_{b_3}$ are monotonic functions with respect to the parameter d_b. Furthermore, $C^*_{m_3}$ and $C^*_{b_3}$ are defined at $k_{pb}(1 - d_g k_{pm}/d_m k_{gb} K_{lb})$ and $k_{pb} + d_m k_{gb} K_{lm}/d_g$, where they are zero, respectively. Therefore, $C^*_{m_3} > 0$, and $C^*_{b_3} > 0$ for all d_b in the interval $I = (k_{pb}(1 - d_g k_{pm}/d_m k_{gb} K_{lb}),\ k_{pb} + d_m k_{gb} K_{lm}/d_g)$. This also implies that $g^*_{b_3} > 0$ in I. Hence, E_3 is a biologically feasible equilibrium and $E_3 \neq E_i$, $i = 0, 1, 2$.

The Jacobian matrix $J(E_3)$ is given by the following matrix:

$$J(E_3) = \begin{pmatrix} -k_{pm} C^*_{m_3}/K_{lm} & 0 & -d_m C^*_{m_3} \\ d_g d_m k_{gb} C^*_{b_3} & -(k_{pb} C^*_{b_3}/K_{lb} + d_m k_{gb} C^*_{m_3}/d_g) & d_m C^*_{m_3} \\ 0 & k_{gb} & -d_g \end{pmatrix}.$$

Hence, the characteristic polynomial of $J(E_3)$ is given by $p(\lambda) = \lambda^3 + b_1\lambda^2 + b_2\lambda + b_3$, where b_1, b_2, and b_3 are defined in Equation (3.4). From $C^*_{m_3} > 0$ and $C^*_{b_3} > 0$, it can be concluded that each $b_i > 0$, $i = 0, 1, 2$.

When $b_1 b_2 - b_3 > 0$ by Routh-Hurwitz criteria, $n = 3$, the roots of $p(\lambda)$ are negative or have negative real part, and therefore, E_3 is locally stable. Next, suppose that $b_1 b_2 - b_3 < 0$. By Descartes'

Rule of Signs, the polynomial $p(\lambda)$ does not have positive roots, since $b_i > 0$, $i = 0, 1, 2$. Therefore, all the roots of $p(\lambda)$ are negative or complex. If all of them are negative, then E_3 is stable, and then, by Routh-Hurwitz criteria $b_1 b_2 - b_3 > 0$, which contradicts the hypothesis. Therefore, $p(\lambda)$ has a negative root, $-\nu$, and two complex conjugate roots, $\mu \pm iw$, since $p(\lambda)$ is of degree three. Notice that $\nu > 0$ and $\mu > 0$. Since, if $\mu < 0$ then E_3 is stable, and then by Routh-Hurwitz criteria $b_1 b_2 - b_3 > 0$, which also contradicts the hypothesis. Therefore, $\mu > 0$, and hence, E_3 is unstable. Finally, if $b_1 b_2 - b_3 = 0$, then $J(E_3)$ has one negative root and two purely imaginary roots given by $-b_1$ and $\pm i\sqrt{b_2}$, where b_1 and b_2 are defined in Equation (3.4), which implies that E_3 is a non-hyperbolic equilibrium point. ∎

4. Bifurcation Analysis

A better insight into the behavior of the system (1)-(3) can be obtained by looking at the bifurcation of each equilibrium point with respect to the parameter d_b, which is varied in the biologically meaningful interval $(0, \infty)$, while fixing all other model parameter values (Wiggins (2003)). Figure 2 shows the bifurcation diagrams for the steady state of the variables C_m^* and C_b^* for the equilibria E_1 (red lines), E_2 (blue lines) and E_3 (black lines) in the case when $b_1 b_2 - b_3 < 0$. The case $b_1 b_2 - b_3 > 0$ leads to similar bifurcation diagrams except for the corresponding lines of the equilibrium E_3 that are solid, since it does not change stability in its parameter domain, and hence, it is omitted here. In addition, the variables for the E_0 are also omitted, since E_0 is unstable for all d_b values. The state-variable g_b^* is also omitted, since its qualitative behaviour is similar to the qualitative behaviour of C_b^*. Notice that Figure 2(b) is a left shift of the bifurcation diagrams presented in Figure 2(a). Since $d_{b_2} = k_{pb}\,(1 - d_g k_{pm}/d_m k_{gb} K_{lb})$ exists only when $d_m k_{gb} K_{lb} > d_g k_{pm}$. Therefore, Figure 2 shows that the system (1)-(3) undergoes a bifurcation at d_{b_1}, k_{pb}, d_{b_2}, and d_{b_3}, where $d_{b_1} = k_{pb} + d_m k_{gb} K_{lm}/d_g$, and d_{b_3} is a root of the polynomial function $b_1 b_2 - b_3$ with respect to d_b such that $d_{b_2} < d_{b_3} < d_{b_1}$.

In addition, the system (1)-(3) undergoes a Hopf-bifurcation at d_{b_3}, when $b_1 b_2 - b_3 < 0$. Due to the complexity of the expressions of E_3 and $J(E_3)$ with respect to d_b for any positive value of d_b, the theoretical proof of the existence of the Hopf-bifurcation at d_{b_3} is omitted. However, from the explicit expression of $b_1 b_2 - b_3$ and from Theorem 3.4, it is easy to prove that the stability of E_3 changes in a neighborhood of d_{b_3}, as the sign of the polynomial function $b_1 b_2 - b_3$ changes in the interval $d_{b_2} < d_b < d_{b_1}$, since either $C_{b_3}^* = 0$ or $C_{m_3}^* = 0$ at d_{b_2} or d_{b_1}, which implies that $b_1 b_2 - b_3 > 0$ in a neighborhood of these parameter values.

Furthermore, it is also easy to prove that $C_{b_2}^* > C_{b_3}^*$ when $d_b < d_{b_2}$ (Figure 2(a) bottom), while $C_{b_3}^* > C_{b_2}^*$ otherwise (Figure 2(a) bottom) or when $d_g k_{pm} > d_m k_{gb} K_{lb}$ (Figure 2(b) bottom). Since the bone formation mainly depends on osteoblasts, the above inequalities can be used in strategies to enhance bone synthesis. For instance, a faster bone formation may be observed under E_2 rather than under E_3 when $d_b < d_{b_2}$. Such inequality implies that the growth factor's concentration is above of the threshold value k_{pm}/d_m, i.e, $g_{b_2}^* = k_{gb} K_{lb}(1 - d_b/k_{pb})/d_g > k_{pm}/d_m$.

Moreover, during bone fracture healing process, the equilibria E_2 represents a successful healing

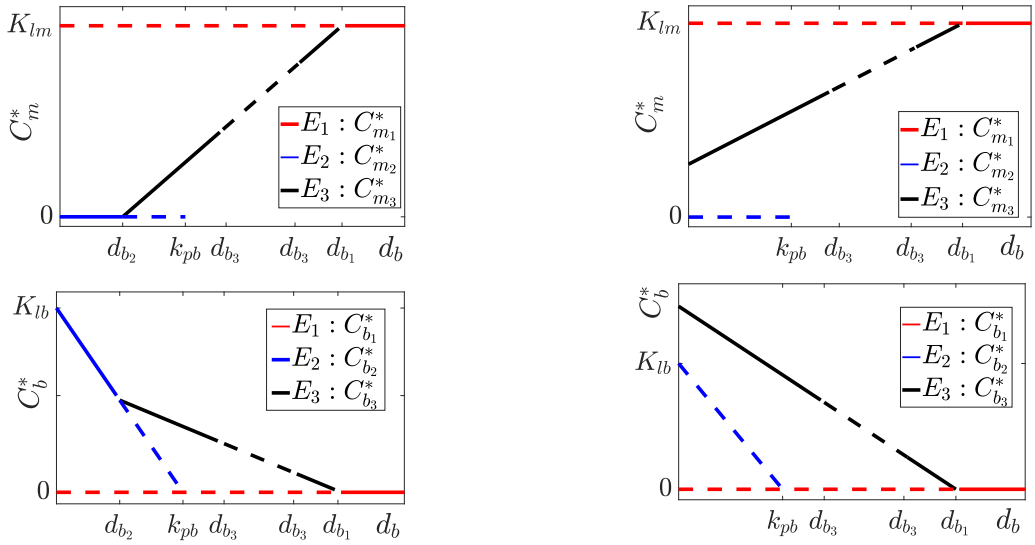

(a) $d_m k_{gb} K_{lb} > k_{pm} d_g$ (b) $d_m k_{gb} K_{lb} < k_{pm} d_g$

Figure 2. Bifurcation diagram of System (1)-(3): solid lines represent stable variables while dashed lines represent unstable variables. E_1 exists for all d_b, E_2 exists when $d_b < k_{pb}$, and E_3 exists when $d_{b_2} < d_b < d_{b_1}$. E_1 changes stability at d_{b_1}, E_2 changes stability at d_{b_2}, and E_3 changes stability at d_{b_3}

outcome (Trejo et al. (2019)). According to Theorem 3.3, E_2 is observed if and only if the proliferation rate of osteoblasts is bigger than their differentiation rate, i.e, $k_{pb} > d_b$, and the growth factor's concentration is above the value given by k_{pm}/d_m. Such results confirm the numerical findings obtained in Bailon-Plaza and Van Der Meulen (2001).

5. Numerical Simulations

In this section a set of numerical simulations is presented to support the theoretical results and to investigate the evolution of the osteoblastogenesis under different therapeutic interventions. According to the qualitative analysis of Model (1)-(3), there are four equilibria: E_0, E_1, E_2, and E_3, where their stability conditions are determined based on the following bifurcation values: k_{pb}, $d_{b_1} = k_{pb} + d_m k_{gb} K_{lm}/d_g$, $d_{b_2} = k_{pb}\left(1 - d_g k_{pm}/d_m k_{gb} K_{lb}\right)$, and d_{b_3} such that $d_{b_2} < d_{b_3} < d_{b_1}$ and d_{b_3} is a root of the polynomial function $b_1 b_2 - b_3$ with respect to d_b.

Table 2. Parameter descriptions and units

Parameter	Description	Range of values	Reference
k_{pm}	Proliferation rate of C_m	$0.5/day$	Trejo et al. (2019)
d_m	Differentiation rate of C_m	$0.1\ (ng/mL)^{-1}/day$	Bailon-Plaza and Van Der Meulen (2001), Trejo et al. (2019)
k_{pb}	Proliferation rate of C_b	$0.2202\ /day$	Bailon-Plaza and Van Der Meulen (2001), Trejo et al. (2019)
d_b	Differentiation rate of C_b	$0.15\ /day$	Bailon-Plaza and Van Der Meulen (2001), Trejo et al. (2019)
k_{gb}	Secretion rate of g_b by C_b	$0.05 - 25\ (ng/cell)/day$	Bailon-Plaza and Van Der Meulen (2001), Moreo et al. (2009)
d_g	Decay rate of g_b	$10 - 100\ /day$	Bailon-Plaza and Van Der Meulen (2001), Moreo et al. (2009)
K_{lb}	Carrying capacity of C_b	$1 \times 10^6\ cells/mL$	Bailon-Plaza and Van Der Meulen (2001)
K_{lm}	Carrying capacity of C_m	$1 \times 10^6\ cells/mL$	Bailon-Plaza and Van Der Meulen (2001)

Table 2 summarizes the baseline parameter values and units for the numerical simulations. These

values are estimated in a qualitative manner from data in other studies (Bailon-Plaza and Van Der Meulen (2001), Moreo et al. (2009), Trejo et al. (2019)), with some being rescaled to account for the different mathematical expressions presented in this work. All simulations are obtained by using the adaptive MATLAB solver `ode23tb` and are initiated with densities of MSCs, osteoblasts, and growth factors set to $C_m(0) = 1000$, $C_b(0) = 1000$, and $g_b(0) = 200$.

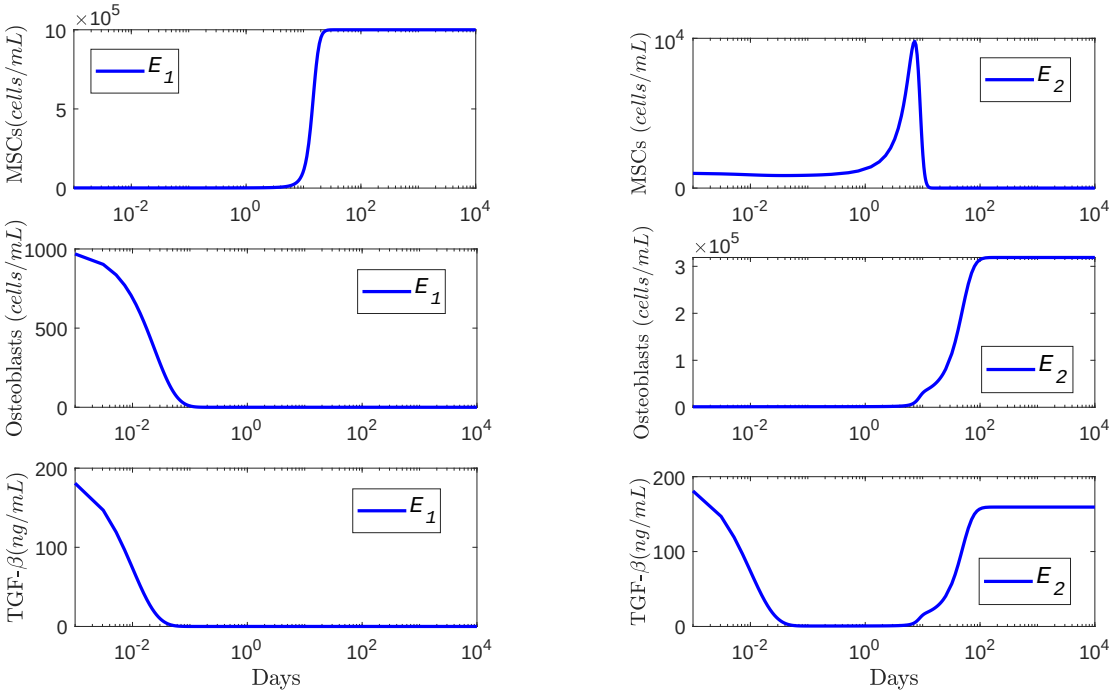

Figure 3. Cellular and molecular evolution for E_1 and E_2, when each of them is stable

Figure 3 shows the time evolution of the MSCs, osteoblasts, and the TGF-β densities of the equilibria E_1 (right) and E_2 (left), when each of them is stable. The simulation in Figure 3 (left) uses $d_b = 51$, and therefore, $d_b > d_{b_1} = 50.2202$, while the simulation in Figure 3 (right) uses $d_b = 0.1$, and therefore, $d_b < d_{b_2} = 0.218$. For the equilibrium E_1, the MSCs maintain a maximum constant density given by their carrying capacity $K_{lm} = 1 \times 10^6$, while the osteoblasts and growth factors densities decay to zero over time. For the equilibrium E_2, the MSCs density decays to zero over time, while the osteoblasts and growth factors maintain constant densities.

The following parameter values are used to show the existence of a Hopf-bifurcation for the model (1)-(3): $K_{lm} = 10000$, $k_{pm} = 0.5$, $d_m = 0.1$, $k_{pb} = 0.2202$, $K_{lb} = 10000$, $d_g = 1$, $k_{gb} = 0.04$. In this case, E_3 has a Hopf-bifurcation value at $d_{b_3} \approx 5.091$. Figure 4 shows the numerical solution for E_3, when E_3 is stable (left): $d_b = 6$, that implies $b_1 b_2 - b_3 \approx 0.905131$, and when E_3 is unstable (right): $d_b = 4$, that implies $b_1 b_2 - b_3 \approx -0.607299$. In Figure 4 (left), the MSCs, osteoblasts, and growth factors densities remain constant over time while in Figure 4 (right), these densities oscillate over time.

Next, the model is used to explore two of the clinical trials, the injection of growth factors and the injection of MSCs (Devescovi et al. (2008), Fakhry et al. (2013)) that have been im-

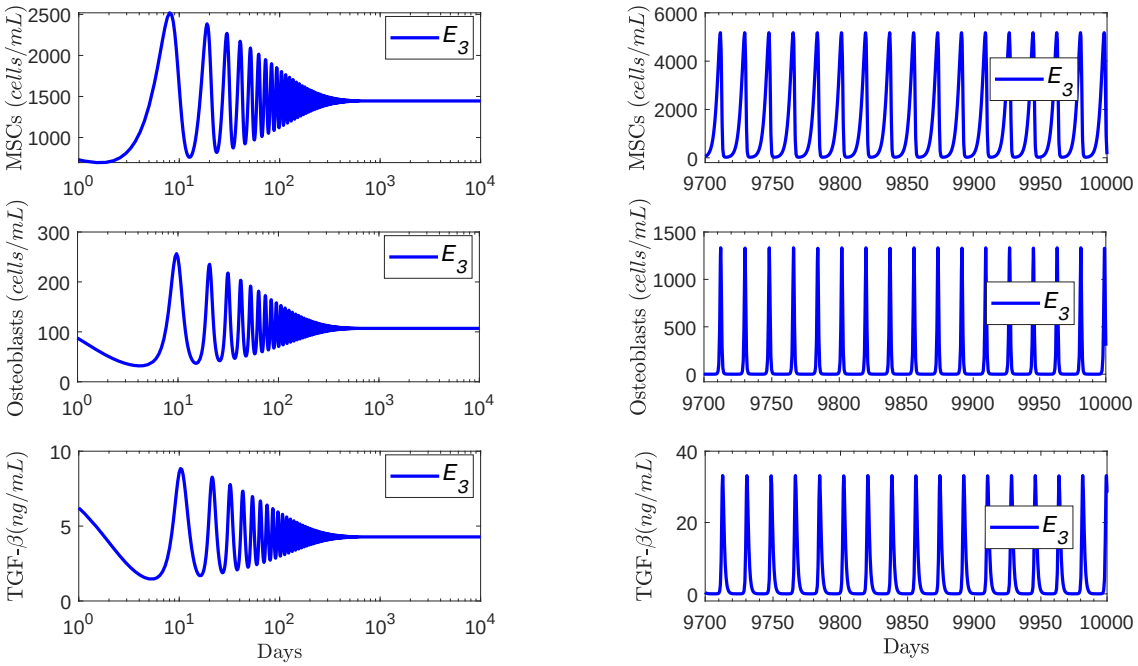

Figure 4. Cellular and molecular evolution for E_3: stable (left) and unstable (right)

plemented in orthopedics to accelerate osteoblastogenesis. The administration of growth-factor drugs is simulated by increasing the production rate of g_b using $k_{gb} = 0.005, 0.05, 0.5$, with $C_m(0) = 1 \times 10^6$. The MSCs injection therapy is simulated by using different initial MSCs densities: $C_m(0) = 1 \times 10^3, 1 \times 10^5, 1 \times 10^6$. The above parameter values correspond to the successful osteogenic outcome E_2.

Figure 5 shows that the administrations of TGF-β and the MSCs are both viable therapeutic interventions, as they each stimulate an earlier increase in the osteoblasts population (middle), driven by corresponding increases in the MSCs differentiation over time (top) and in the growth factor concentrations (bottom).

6. Discussion and Conclusion

The presented model was used to study the fundamental mechanisms of mesenchymal stem cell differentiation towards osteoblasts by taking into account the growth factors stimuli directing the osteoblastogenesis process. The corresponding mathematical findings revealed that there are two possible successful outcomes, E_2 and E_3, which are observed when $d_b < k_{pb} + d_m k_{gb} K_{lm}/d_g$, depending on the MSCs differentiation site (Lin et al. (2019), Via et al. (2012)). Moreover, the osteoblastogenesis process evolves to the equilibria E_2 when the growth factor concentration is above the growth factor's concentration value given by k_{pm}/d_m (Theorem 3.3). Otherwise, the osteoblastogenesis results in E_3 (Theorem 3.4).

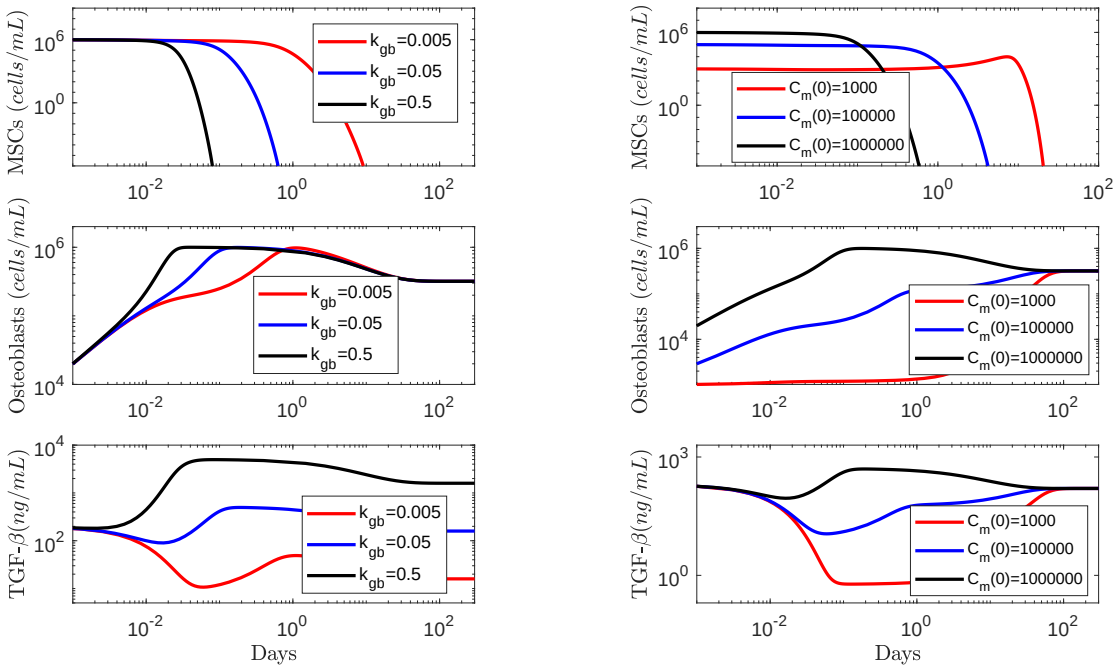

Figure 5. Cellular and molecular evolution of the osteoblastogenesis under the administration of growth factors (left) and MSCs injection (right)

Furthermore, since in a successful osteoblastogenesis, it is expected that MSCs, osteoblasts, and growth factors remain at constant densities over time, then E_3 under the conditions $d_{b_2} < d_b < d_{b_1}$ and $b_1 b_2 - b_3 < 0$ represents a pathological successful osteogenic differentiation. In this case, the state-variables of E_3 may never achieve a constant-steady state value, as seen in Figure 4 (right). Additionally, it can be concluded, from the stability and bifurcation analysis of the model, that when the proliferation rate of osteoblasts is bigger than their differentiation rate, i.e, $k_{pb} > d_b$, and the growth factors concentration is above the growth factor's concentration value given by k_{pm}/d_m, then a faster bone formation would be observed under E_2 rather than under E_3 variables. Conversely, a faster bone formation would be observed under E_3 rather than under E_2 when the growth factors concentration is below the growth factor's concentration value given by k_{pm}/d_m, ensuring that $d_{b_2} < d_b < d_{b_1}$ and $b_1 b_2 - b_3 > 0$.

The numerical simulations show that growth factors and MSCs therapeutic interventions are both feasible orthopaedic strategies to accelerate bone formation. The model can also be easily adapted to other therapeutic approaches, such as the administration of other molecular agents that stimulate the osteogenic process. Next, we plan to extend the model by incorporating the growth factor stimulus in the cellular migration, proliferation, and differentiation processes, which will allow for a better understanding of the regulatory effects of growth factors in tissue formation.

Acknowledgment:

This work was supported by the Mexican National Council of Science and Technology (CONACyT) and the University of Texas at Arlington.

REFERENCES

Bailon-Plaza, A. and Van Der Meulen, M.C. (2001). A mathematical framework to study the effects of growth factor influences on fracture healing, Journal of Theoretical Biology, Vol. 212, No. 2, pp. 191–209.

Carlier, A., Geris, L., Van Gastel, N., Carmeliet, G. and Van Oosterwyck, H. (2015). Oxygen as a critical determinant of bone fracture healing-a multiscale model, Journal of Theoretical Biology, Vol. 365, pp. 247-264.

Devescovi, V., Leonardi, E., Ciapetti, G. and Cenni, E. (2008). Growth factors in bone repair, La Chirurgia degli organi di movimento, Vol. 92, No. 3, pp. 161-168.

Dimitriou, R., Tsiridis, E. and Giannoudis, P.V. (2005). Current concepts of molecular aspects of bone healing, Injury, Vol. 36, No. 12, pp. 1392–1404.

Doblaré, M., García, J.M. and Gómez, M.J. (2004). Modelling bone tissue fracture and healing: a review, Engineering Fracture Mechanics, Vol. 71, No. 13, pp. 1809–1840.

Fakhry, M., Hamade, E., Badran, B., Buchet, R. and Magne, D. (2013). Molecular mechanisms of mesenchymal stem cell differentiation towards osteoblasts, World Journal of Stem Cells, Vol. 5, No. 4, pp. 136.

Florencio-Silva, R., Sasso, G.R.D.S., Sasso-Cerri, E., Simões, M.J. and Cerri, P.S. (2015). Biology of bone tissue: structure, function, and factors that influence bone cells, BioMed Research International, Vol. 2015.

Garg, P., Mazur, M.M., Buck, A.C., Wandtke, M.E., Liu, J. and Ebraheim, N.A. (2017). Prospective review of mesenchymal stem cells differentiation into osteoblasts, Orthopaedic Surgery, Vol. 9, No. 1, pp. 13–19.

Ghiasi, M.S. and Chen, J., Vaziri, A., Rodriguez, E.K. and Nazarian, A. (2017). Bone fracture healing in mechanobiological modeling: A review of principles and methods, Bone Reports, Vol. 6, pp. 87–100.

Lin, H., Sohn, J., Shen, H., Langhans, M.T. and Tuan, R.S. (2019). Bone marrow mesenchymal stem cells: Aging and tissue engineering applications to enhance bone healing, Biomaterials, Vol. 203, pp. 96–110.

Moreo, P., García-Aznar, J.M. and Doblaré, M. (2009). Bone ingrowth on the surface of endosseous implants, Part 1: Mathematical model, Journal of Theoretical Biology, Vol. 260, No. 1, pp. 1–12.

Trejo, I., Kojouharov, H. and Chen-Charpentier, B. (2019). Modeling the macrophage-mediated inflammation involved in the bone fracture healing process, Mathematical and Computational Applications, Vol. 24, No. 1, pp. 12.

Via, A.G., Frizziero, A. and Oliva, F. (2012). Biological properties of mesenchymal stem cells from different sources, Muscles, Ligaments and Tendons Journal, Vol. 2, No. 3, pp. 154.

Wiggins, S. (2003). *Introduction to Applied Nonlinear Dynamical Systems and Chaos*, Springer Science & Business Media.

Wu, M., Chen, G. and Li, Y.P. (2016). TGF-β and BMP signaling in osteoblast, skeletal development, and bone formation, homeostasis and disease, Bone research, Vol. 4, pp. 16009.